

Explore methods to enhance the properties of RAC through the addition of supplementary cementitious materials (e.g., fly ash, silica fume) and advanced mixing techniques.

Abhay Yadav¹, Satish Parihar²

Department of Civil, FET, Rama university Uttar Pradesh Kanpur 209217

Email id: abhayumiitm1819@gmail.com

Abstract:

The elevated porosity of recycled coarse aggregate renders recycled aggregate concrete (RAC) more susceptible to freeze-thaw (FT) damage and chemical degradation, significantly hindering the industrial use of RAC in civil engineering. This research reports an experimental investigation into the synergistic effects of freeze-thaw damage and sulphate assault on the mechanical properties of high-performance recycled aggregate concrete. The impact of combined damage on the mass, solution-filled pore volume, dynamic elastic modulus, compressive strength, splitting tensile strength, and fracture energy of recycled aggregate concrete (RAC) was examined. The results indicated that water-exposed freeze-thaw cycles lead to greater deterioration in mass loss, elastic modulus, and compressive strength, whereas sulphate-exposed freeze-thaw cycles exhibit more pronounced degradation in splitting tensile strength and fracture energy. Furthermore, the decline in splitting tensile strength is more pronounced than that in compressive strength. The peak losses in compressive and splitting tensile strength were 28.7% and 35%, respectively. The fracture energy exhibited an upward trend until 60 FT cycles, subsequently declining to 180 FT cycles. The fracture energy demonstrates a maximum increase of around 45% and 39% for samples exposed to water and sulphate, respectively, after undergoing 60 freeze-thaw cycles. The examination of failure modes in coarse aggregate has demonstrated that FT damage leads to a substantial decline in the adhesive strength of mortar. Following 180 FT cycles, the area percentage of pulled-out failure rose from 7.3% to over 17.3%.

Keywords: Recycled aggregate concrete; freeze-thaw resistance; sulphate degradation; strength; fracture energy

1. Introduction

Concrete, as the most prevalent construction material, significantly contributes to the depletion of natural resources and global greenhouse gas emissions [1,2]. Recycled coarse aggregate (RCA) is a promising sustainable construction material for effective waste management. Despite rapid advancements in research concerning the recycling of construction and demolition debris, many countries find the outcomes unsatisfactory due to the poorer properties of recycled aggregate concrete compared to conventional concrete. Numerous research have been conducted in recent years to enhance the mechanical qualities of Recycled Aggregate Concrete (RAC) by the use of chemical admixtures, active mineral additions, and fibres [6–8]. Bui et al. [9] investigated the characteristics of RAC utilising a novel combination approach, wherein only large-sized recycled aggregate particles were substituted with conventional aggregate in coarse aggregates. The research established that the substantial coarse aggregate is essential for the performance of recycled aggregate concrete (RAC). Employing the novel combination process, the proportion of recycled coarse aggregate in the concrete may reach 50%, with just a minor alteration in compressive strength observed. the standard concrete. Bravo et al. [10] examined the efficacy of the superplasticizer on the mechanical properties of recycled aggregate concrete (RAC) and validated the effectiveness of polycarboxylic superplasticizer in improving the mechanical properties of RAC to an acceptable standard.

Enhancing the characteristics of mortar and interfacial transition zones (ITZs) could substantially augment the mechanical qualities of recycled aggregate concrete (RAC). Nonetheless, the substandard characteristics of RCA, including elevated porosity, significant water absorption, reduced density, and diminished strength, persist. Pepe et al. [11] determined that the mechanical performance of recycled aggregate concrete (RAC) could be forecasted just by evaluating the water absorption capacity to assess the "quality" of recycled coarse aggregate. Dilbas et al. [12] examined the permeability of RAC and noted a substantial decrease in its permeability upon the incorporation of 10% silica fume into the concrete mixture. Conversely, fluid infiltration is a principal element affecting freeze-thaw damage in concrete and remains a significant durability issue for this material [13]. When the water saturation level surpasses 86–88%, freeze-thaw damage becomes unavoidable, regardless of air entrainment, even after only a few freeze-thaw cycles [14].

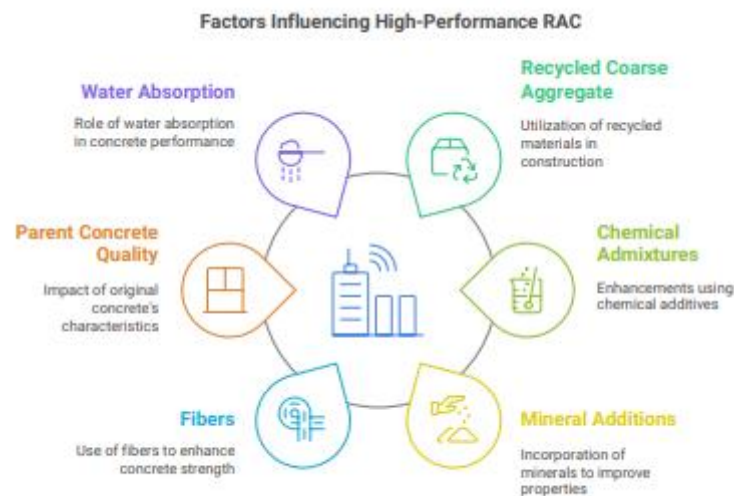


Figure: 1 Factor influencing high performance RAC

The elevated porosity of recycled coarse aggregate leads to increased water absorption and diminished resistance to chemical assaults relative to conventional concrete. Kou and Poon [15] investigated the influence of parent concrete quality on the characteristics of recycled aggregate concrete (RAC) and observed an elevation in chloride-ion penetration when recycled coarse aggregate was utilised, in contrast to conventional concrete. The sulphate resistance of concrete incorporating recycled coarse aggregate and natural aggregate was also validated through evaluation [16]. Significant study has been undertaken regarding the durability of RAC in relation to freeze-thaw cycles and sulphate assault [17–19]. Relatively few research have been conducted on the synergistic effects of chemical assaults (chloride corrosion, sulphate attack) and freeze-thaw damage [20–23]. Farnam et al. [24] investigated the damage progression in concrete subjected to deicing salt and found that ice formation was the primary cause of damage in mortar exposed to low concentrations of $MgCl_2$ solutions (<10% by weight), whereas deterioration at higher concentrations ($\geq 10\%$ by weight) was likely attributable to chemical attacks.

China possesses the third largest area of saline-alkali land globally. Saline-alkali lands are predominantly situated in the northwestern regions of China, including Xinjiang, Ningxia, and Inner Mongolia, as well as northeastern China. Many of these places are distinguished by elevated altitude/latitude and low winter temperatures. Thus, the cumulative damage is more pertinent to operational situations than the traditional FT cycles and sulphate immersion assessments. The sulphate attack on concrete is influenced by numerous factors.

Thaumasite is more prone to develop at low temperatures of approximately 5 °C, resulting in a diminished binding capacity of cement. Extensive experimental study has been conducted on the

mechanical characteristics and durability of RAC under freeze-thaw cycles and sulphate assaults. Furthermore, efforts have been undertaken to investigate the synergistic effects of chemical assaults and FT damage on conventional concrete. Nonetheless, there is a paucity of published research concerning the impact of sulphate attack and freeze-thaw degradation on the tensile and fracture parameters of recycled aggregate concrete (RAC). This study aims to examine the impact of combined freeze-thaw damage and sulphate assault on the mechanical properties of high-performance recycled aggregate concrete (RAC). The study examined the impact of combined damage on mass, solution-filled pore volume, dynamic elastic modulus (Edym), compressive strength, splitting tensile strength, and fracture energy of recycled aggregate concrete (RAC). The mid-span fracture surface of prisms was examined to gain insight into the failure mode of the aggregate concerning freeze-thaw degradation. Additionally, XRD investigations were conducted on RAC subjected to simultaneous FT damage and sulphate assault. This study yields significant results and analyses about the prospective application of high-performance RAC in cold climates.

2. Materials and Methods

2.1 Specimens of materials

The parameters of the RAC combination are presented in Table 1. Recycled Concrete Aggregate (RCA) was generated from crushed and sieved leftover pavement concrete obtained during pavement rehabilitation. The dimensions of recycled coarse aggregate and natural coarse aggregate (NCA) ranged from 4.75 mm to 19 mm, whereas the water absorption ratio of recycled coarse aggregate (RCA) was 8.5%. Fly ash (FA), constituting 20% of the weight of the gelatinising agent, was utilised as a substitute for cement and as an active mineral ingredient in this context. Figure 1 illustrates the gradation curves of fly ash, fine aggregate, natural coarse aggregate (NCA), and recycled coarse aggregate (RCA). Furthermore, a polycarboxylic superplasticizer (SP) was employed to enhance the workability of recycled aggregate concrete (RAC). The characteristics of the polycarboxylic superplasticizer are presented in Table 2. Both FA and SP were employed to enhance the mechanical qualities of RAC.

Prior to casting, the RCA was submerged in water for three days to achieve saturation. Following casting, all specimens were immersed in water at 20 °C for a duration of three months; hence, the strength attained during the ensuing testing period can be disregarded.

Table 1. Mix properties of concrete (kg·m⁻³)

Cement	Sand	NCA	RCA	FA	SP	Water	w/c	w/b
440	610	620	620	110	1.1	165	0.5	0.4

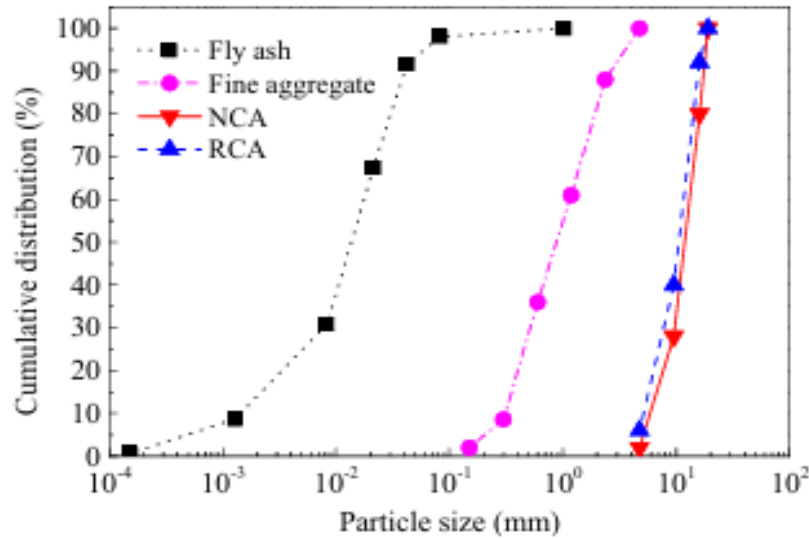


Figure 1. The gradation curves for fly ash, fine aggregate, NCA and RCA.

Table 2. Properties of the polycarboxylic superplasticizer.

Appearance	Water-Reducing Ratio	Moisture Content	Bulk Density/kg.m ⁻³
Grey powder	≥25%	≤5.0%	500~700
PH Value (20 °C, 10% Aqueous Solutions)	Chloride Ions Content	Sodium Sulfate Content	Alkali Content
6~8	≤0.03%	≤3.0%	≤0.5%

In accordance with the Standard Test Method GB/T 50082-2009 [30], beam specimens of 100 mm × 100 mm × 400 mm were utilised in the FT tests. Thus, a notched beam of identical dimensions was utilised to examine the fracture behaviour of RAC following exposure to 60, 90, 120, 150, and 180 freeze-thaw cycles. In the three-point bending test, the span-to-depth ratio was 3, and the notch-to-depth ratio was 0.3 (Figure 2).

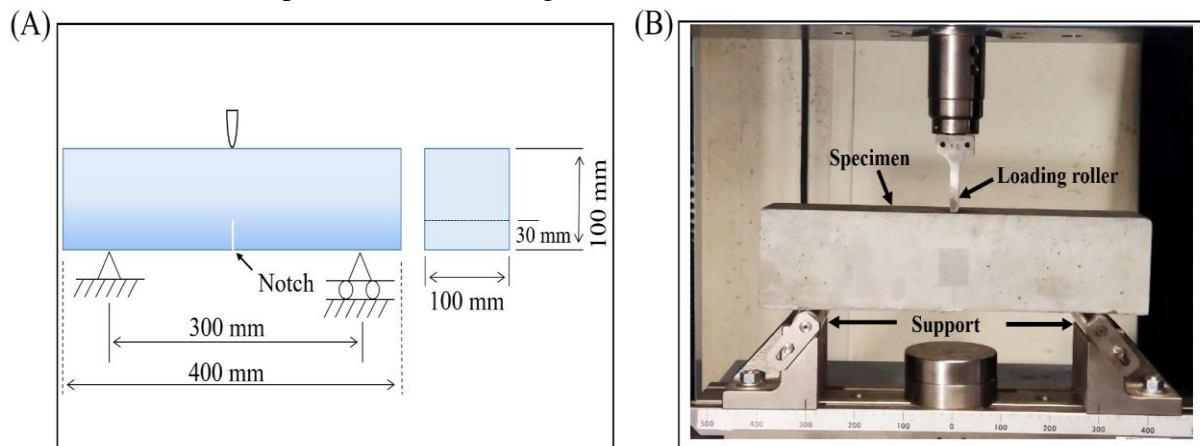


Figure 2. Schematic of the notched beam (A) and experimental apparatus of the notched beam (B) under quasi-static three-point bending test.

2.2 Freeze-Thaw Tests

Rapid freeze-thaw experiments were performed on specimens saturated with water or sulphate solution utilising a rapid freeze-thaw testing apparatus. As per GB/T 50082-2009 [30], the internal temperature of specimens was regulated to fluctuate between 5 ± 2 °C and -15 ± 2 °C during a duration of approximately 4 hours for each cycle. The cycle commenced at 5 °C and decreased to -15 °C over 2 hours, succeeded by a 10-minute isothermal phase at -15 °C. The temperature was elevated to 5 °C during a duration of 1.5 hours and sustained for an additional

10 minutes. Figure 3 illustrates the interior temperature of specimens undergoing freezing and thawing.

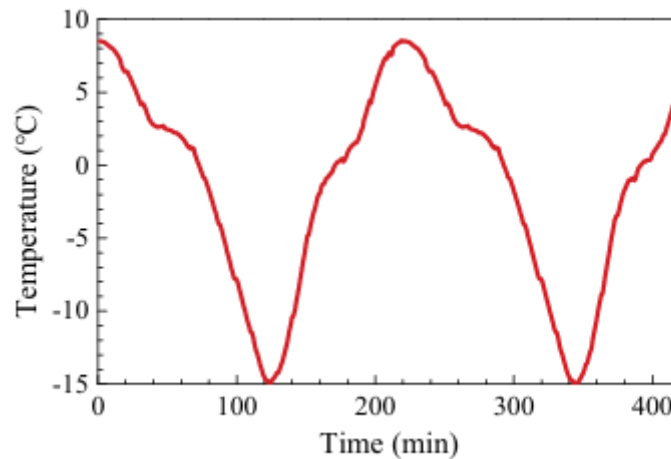


Figure 3. Internal temperature of notched beam in freeze–thaw cycles

2.3 Mass Change, Water Absorption and Internal Damage

Prior to freeze–thaw testing, the specimens were dehydrated in a drying oven at 60 °C for 24 hours. This comparatively low temperature was chosen to prevent any damage to the pore structure at elevated temperatures [31] and to mitigate the impact of the drying process on the specimens' water absorption. The subsequent step involved measuring the oven-dried bulk and Edym. The specimens were submerged in a sulphate solution (or water) for one week [32] as a pre-saturation phase; thereafter, the saturated surface dry mass was documented. The natural saturated specimens were subsequently exposed to 60, 90, 120, 150, and 180 freeze-thaw cycles, during which they were immersed in water or a sulphate solution. A 5% (by mass) sodium sulphate solution was utilised in this work as the sulphate solution. Following FT testing, the saturated mass, oven-dried mass, and Edym were re-evaluated to assess frost damage. The mass loss (percentage) of concrete specimens induced by freeze-thaw cycles can be calculated by

$$\Delta m_N = (m_1 - m_2)/m_1 \times 100\% \quad (1)$$

where m_1 (g) and m_2 (g) represent the mass prior to and subsequent to N freeze–thaw cycles, respectively.

Micro-cracks formed throughout FT cycles, creating additional pathways for the solution to infiltrate the interior pores. Thus, saturated water absorption serves as an indirect method to assess the formation of micro-cracks [33,34], which was also employed in this study to evaluate FT damage. The volume of solution-filled pores and voids (V , mm^{-3}) was determined from the saturated mass (m_s , g) and the oven-dried mass (m_d , g) utilising Equation (2):

$$V = (m_s - m_d)/\rho \quad (2)$$

where ρ ($\text{g} \cdot \text{mm}^{-3}$) is the density of water.

The extent of internal damage caused by freeze–thaw cycles can be regularly evaluated by a relative dynamic elastic modulus (RDEM). Here, a damage parameter (1-RDEM) was used to assess the frost damage, which can be expressed by Equation (3):

$$D = 1 - E_{dyn,FT}/E_{dyn,0} \quad (3)$$

where $E_{dyn,0}$ (GPa) and $E_{dyn,FT}$ (GPa) are the dynamic elastic modulus before and after FT cycles.

2.4 Mechanical properties Tests

Three-point bending tests (TPBT), as outlined by the RILEM Technical Committee 50-FMC [35], were performed utilising a 100 kN electronic universal testing equipment (SHIMADZU). The beam specimen was 100 mm x 100 mm x 400 mm. The notched specimens were subjected to loading until failure at a crosshead displacement rate of 0.1 mm per minute. An electro-hydraulic testing machine with a capacity of 2000 kN was utilised for compression and splitting tests. As per GB/T 50081-2002 [36], the stress rates were established at $0.5 \text{ MPa} \cdot \text{s}^{-1}$ for compression testing and $0.05 \text{ MPa} \cdot \text{s}^{-1}$ for splitting tests. The cubic specimens were sectioned to dimensions of 100 mm x 100 mm x 100 mm from the shattered prism specimens to guarantee that the resultant compression and splitting tensile results were derived from concrete materials with identical attributes [37]. The shear forces near the supports during the bending test were all below 4 kN, indicating minimal impact on the measured strength of the cubic specimens. The breakdown energy of concrete, G_F , is a crucial metric that signifies its resistance to cracking in fracture mechanics and crack analysis. It is defined as the energy necessary to generate a unit area of a fracture. In accordance with the RILEM [35] guidelines, fracture energy can be calculated from the experimental load-deflection curve use Equation (4):

$$G_F = (W_0 + mg\delta_0)/A \quad (4)$$

where W_0 is the total area under the load-deflection curve, m is the mass of the beam between the supports, δ_0 is the mid-span deflection of the beam upon failure, $g = 9.81 \text{ m} \cdot \text{s}^{-2}$ is the gravitational acceleration and A is the area of the ligament. Here, $A = t \cdot h$, where t is the width of the beam and h (equal to 70 mm) is the depth of the ligament.

3. Results and Discussion

The impact of FT damage on physical parameters such as mass loss, water absorption, and dynamic elastic modulus was examined. The results from the TPBT, compression tests, and splitting tests are subsequently discussed, followed by the XRD analysis.

3.1 Mass Loss and Water Absorption

Previous investigations [14,22] indicate that the normalised water absorption is related to the square root of time, with a slope ranging from 0.026 to 0.033 after 7 days of immersion in water [14]. Consequently, the alteration in water absorption seen in this study may be attributed to FT damage.

Table 3 presents the documented masses and computed solution-filled pore volumes under various FT cycles and exposure circumstances. Figure 4 illustrates the computed mass losses for saturated and oven-dried conditions across various FT cycles. Saturated and oven-dried specimens subjected to water exhibit greater mass loss than those treated to sulphate solution. This outcome suggests that freeze-thaw cycles with water exposure may inflict greater damage on the concrete. Nevertheless, the mass loss due to oven drying (Figure 4B) for both specimen groups escalated with the rise in freeze-thaw (FT) cycles, aligning with the damage buildup resulting from the higher FT cycles. Nonetheless, the saturated mass loss (Figure 4A) remained unsteady throughout the FT tests. This suggests that oven-dried tests are more appropriate for evaluating FT damage than the saturated mass method.

Table 3. Mass and solution-filled pore volume of notched beams subjected to freeze–thaw cycles.

Specimen	FT Cycles	m_{1s} (g)	m_{1d} (g)	m_{2s} (g)	m_{2d} (g)	V_1 (mm ³)	V_2 (mm ³)
0 (W0/S0)	0	-	-	-	-	-	-
W60	60	9306	9217	9270	9178	89	92
W90	90	9087	8999	9023	8931	88	92
W120	120	9539	9474	9474	9399	65	75
W150	150	9101	9018	9041	8924	83	117
W180	180	9047	8955	8976	8813	92	163
S60	60	9143	9048	9116	9029	95	87
S90	90	9298	9224	9273	9205	74	68
S120	120	9106	9019	9083	8985	87	98
S150	150	9060	8996	9031	8944	64	87
S180	180	9206	9127	9146	9033	79	113

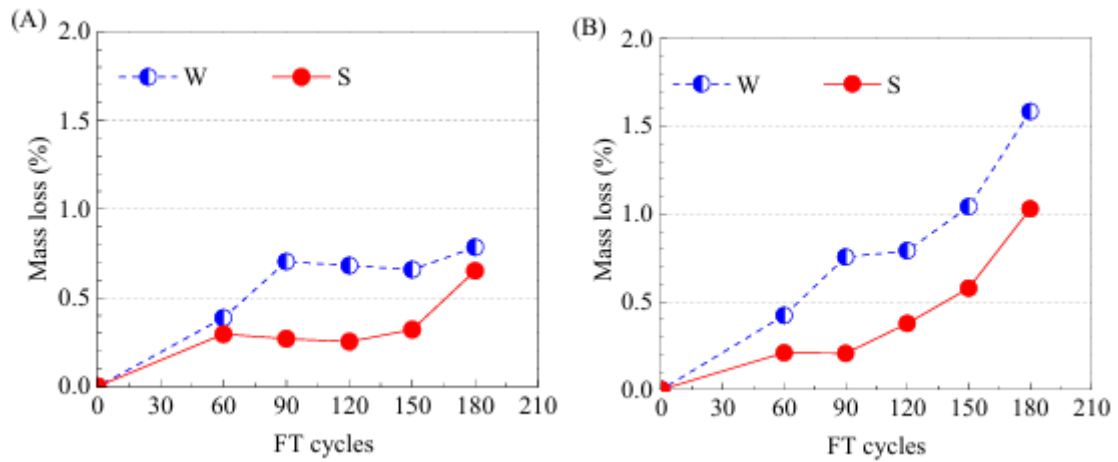


Figure 4. Saturated mass loss (A) and oven-dried mass loss (B) at different FT cycles of water saturated (W) and sulfate attack (S) RAC.

Furthermore, FT induces the formation of micro-cracks, ultimately leading to alterations in solution absorption [33]. Figure 5 illustrates the relative solution-filled pore volume, defined as the ratio of the solution-filled pore volume post-FT cycles to that before FT cycles. For water-exposed specimens (W), the relative solution-filled pore volume consistently exceeded one, so confirming that FT leads to an augmentation in solution-filled pore volume. A comparable effect was observed in sulfate-exposed specimens (S) following exposure to 120 FT cycles or more. Nonetheless, for specimens subjected to sulphate, there was minimal reduction in pore volumes from 60 to 90 freeze-thaw cycles. This may be ascribed to the precipitation of synthesised ettringite and thaumasite, a prevalent occurrence of sulphate attack, leading to a reduction in pore volume [38–40].

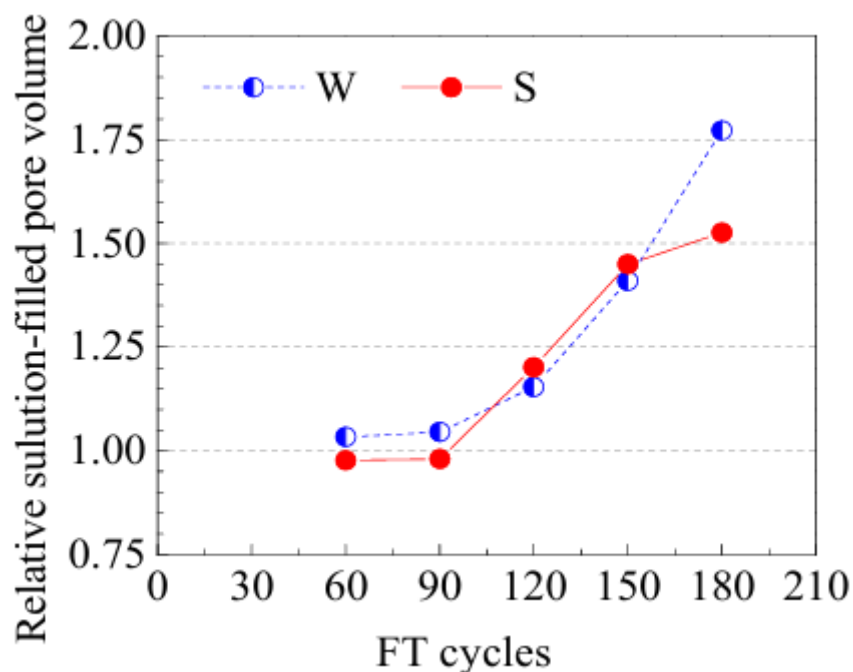


Figure 5. Changes of solution-filled pore volume of water-exposed (W) and sulfate-exposed (S) RAC samples at different freeze-thaw cycles.

In contrast to mass loss, the variation in solution-filled pore volume between specimens exposed to water and sulphate was minimal at lower freeze-thaw cycles, but 180 cycles led to a 16.1%

increase in pore volume in the water-exposed sample (Figure 5). For specimens exposed to 120 and 150 FT cycles, the pore volume alterations in the sulphate solution exposure group were slightly greater (4.1% and 2.9%, respectively) than those in the water exposure group. A minor degree of spalling due to salt crystallisation during oven-drying results in a reduced dried bulk and may have contributed to this tendency.

3.2 Dynamic Elastic Modulus

The computed damage characteristics under various FT cycles and exposure conditions are presented in Table 4. Figure 6 illustrates the impact of several FT cycles on the damage parameter of samples subjected to water and sulphate. For RAC, specimens exposed to water during freeze-thaw cycles exhibited significantly worse deterioration of elastic modulus across all examined freeze-thaw cycles compared to those exposed to sulphate. Specimens exposed to water and sulphate experienced maximum reductions in elastic modulus (damage parameters) of 24.6% and 21.5%, respectively, after undergoing 180 freeze-thaw cycles. For water-exposed specimens subjected to 120 or fewer freeze-thaw cycles, the damage parameter progressively increased with the number of cycles. However, upon undergoing 120 or more cycles, the progression of the damage parameter exhibited a declining trend. In contrast to the water-exposed specimens, the damage parameter of sulphate-exposed specimens exhibited an opposing trend.

Table 4. Metallurgical characteristics of notched beams exposed to freeze–thaw cycles.

Specimen	FT Cycles	D	f_c (MPa)	f_t (MPa)	G_F ($\text{J}\cdot\text{mm}^{-2}$)
0 (W0/S0)	0	0	59.5	4.0	300.9
W60	60	0.068	56.2	3.5	437.1
W90	90	0.109	51.1	3.2	326.7
W120	120	0.173	47.5	3.0	342.5
W150	150	0.211	44.3	2.9	309.2
W180	180	0.246	42.4	2.6	274.1
S60	60	0.048	57.8	3.6	417.9
S90	90	0.073	53.5	3.3	386.1
S120	120	0.092	51.2	3.1	322.2
S150	150	0.15	49.8	3.0	252.1
S180	180	0.215	46.1	2.6	254.1

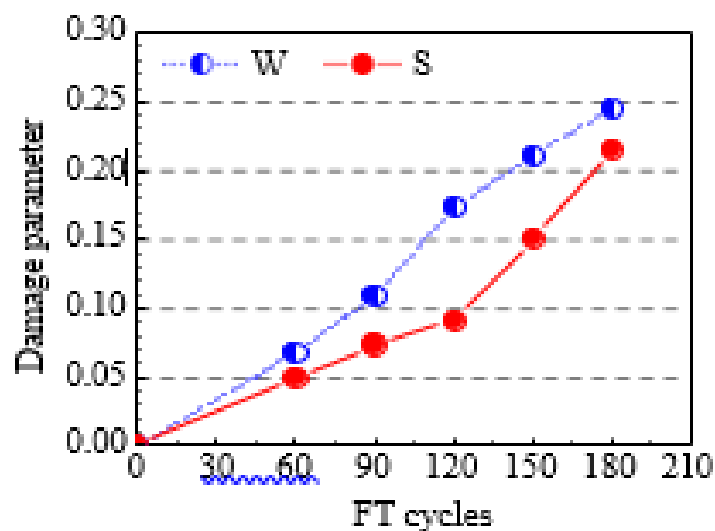


Figure 6. Progressions of the damage parameter for water-exposed (W) and sulphate-exposed (S) recycled aggregate concrete (RAC) samples across several freeze-thaw cycles.

The specimen given a dicing saltwater solution exhibited a more pronounced decline in elastic modulus, attributed to the differential liquid pressure induced by the water and salt solution [21,24]. Furthermore, the research by Zeng et al. [21] shown that sodium chloride in solution

reduces ice formation, thereby leading to a drop in maximum liquid pressure. Sodium sulphate may exert comparable effects on pore pressure in relation to the dicing salt.

3.3 Compressive Strength and Splitting Tensile Strength

To comprehend the deterioration of strength throughout several freeze-thaw cycles, assessments of both compressive strength and splitting tensile strength were conducted. The recorded strengths during various FT cycles and exposure settings are presented in Table 4. Figure 7A illustrates the dimensionless strength values, namely the relative residual compressive and splitting tensile strength, in relation to FT cycles.

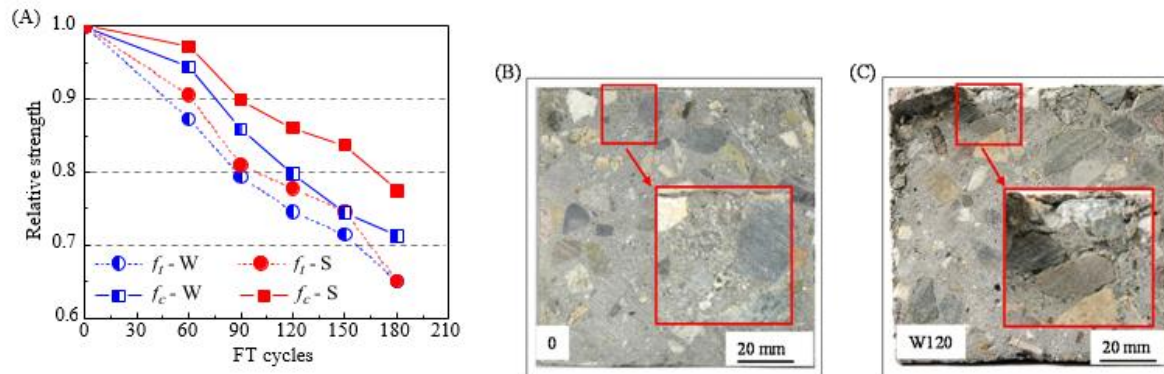


Figure 7. Changes in residual strength (A) and interfacial transition zones (B,C) during several freeze-thaw cycles.

In RAC exposed to sulphate freeze-thaw damage, the reduction in compressive strength was less significant than that observed in specimens subjected to water freeze-thaw damage. Samples exposed to water and sulphate and subjected to 180 freeze-thaw cycles exhibited residual compressive strengths of around 71% and 78% of their original strength, respectively. The residual strength of W180 was approximately 92% of that of S180. This phenomenon was corroborated by Jiang [41] through an examination of the durability of high-performance cement under identical exposure conditions.

Furthermore, both the recycled aggregate concrete (RAC) in this work and the high-performance concrete ($w/c = 0.56$) referenced in [41], when exposed to freeze-thaw cycles, exhibited a significant linear correlation between their compressive strengths and the number of freeze-thaw cycles. Furthermore, due to its elevated porosity, the RCA concrete exhibited a greater reduction in compressive strength relative to regular concrete in [41], although utilising a lower water-to-binder ratio.

Nonetheless, minor variations were seen in the splitting tensile strength of RAC subjected to varied exposure circumstances in this investigation. For samples exposed to both water and sulphate during 180 freeze-thaw cycles, the residual splitting tensile strength was approximately 65% of the initial strength. For RAC exposed to sulfate-FT damage, the reduction in splitting tensile strength was less significant than that of specimens subjected to water-FT damage, even after 180 FT cycles.

Following exposure to 180 freeze-thaw cycles, a reduction of around 35% in splitting tensile strength was observed, surpassing the decline in compressive strength. Consequently, in comparison to compressive strength, tensile strength exhibits more sensitivity to FT damage. The interfacial connection between aggregate and mortar is crucial for tensile strength. Figure 7B,C illustrates the cutting surface of the control specimen (0) and the water-exposed specimen subjected to 120 freeze-thaw cycles (W120). In the FT-damaged specimen, macrocracks were seen mostly in surface-adjacent locations at the interface between the aggregate and mortar. Consequently, damage in the interfacial transition zones (ITZs) also transpires during cyclic freeze-thaw damage, exacerbating the deterioration of splitting tensile strength. The subsequent part will address the quantitative examination of the degradation in ITZs.

3.4 Fracture Energy

Figure 8A illustrates the normalised fracture energy in relation to FT cycles, derived by dividing the GF by the control. In contrast to the loss observed in Edyn and the strength reduction under FT damage, both water- and sulphate-exposed samples exhibited an increase in fracture energy. The fracture energy exhibited an increasing trend up to 60 FT cycles, subsequently demonstrating an overall decline until 180 FT cycles. Following exposure to 60 FT cycles, the fracture energy exhibited a maximum increase of approximately 45% for water-exposed samples and 39% for sulphate-exposed samples. The fracture energy of sulphate-exposed specimens decreases more significantly than that of water-exposed specimens. Following 180 FT cycles, the sulphate-exposed specimen exhibited a reduction in fracture energy of approximately 16%, surpassing the 9% decrease observed in the water-exposed specimen. Kazberuk et al. [42] observed a comparable variation trend in their investigation of the impact of internal frost damage on the fracture energy of both aerated and non-aerated concrete.

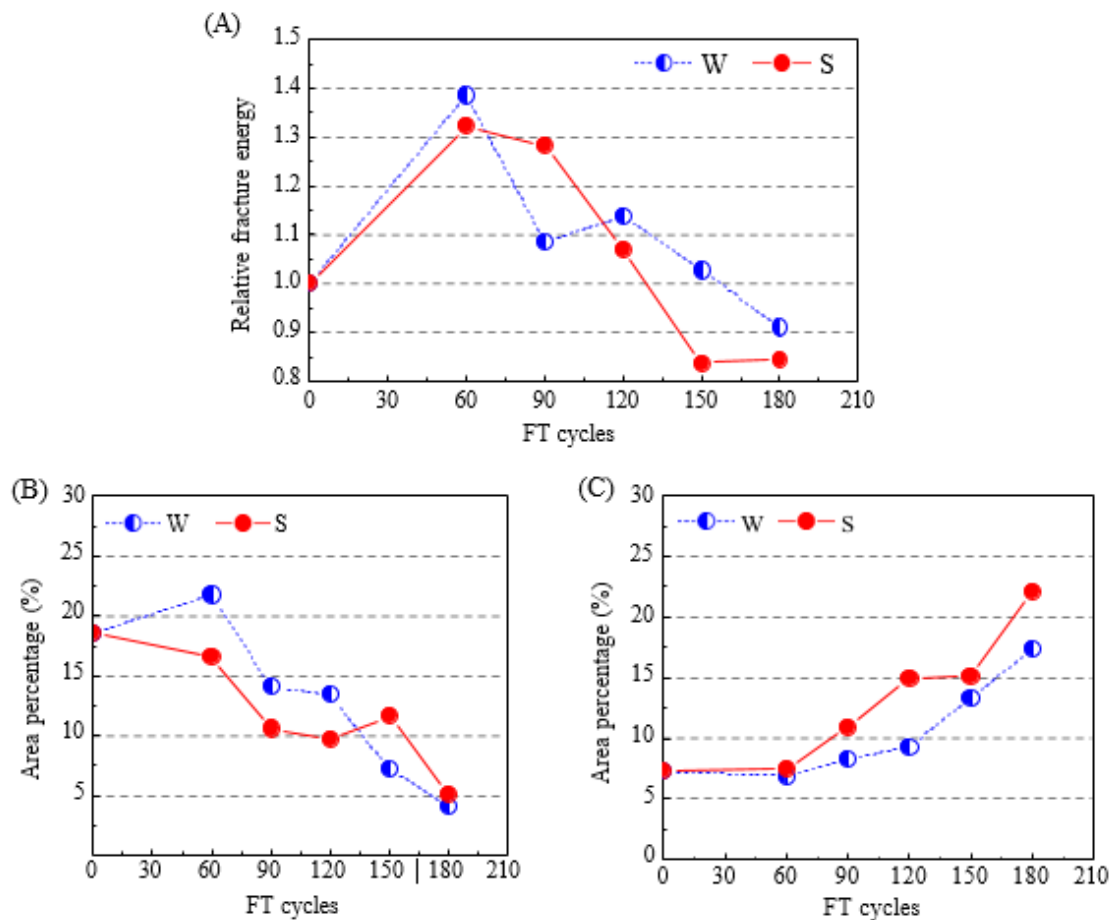


Figure 8: Changes in fracture energy (A), area percentage of pulled-out failure (C), and aggregate splitting failure (B) during various FT cycles.

The fracture energy, G_F , required for the creation of a fracture surface can be expressed as

$$G_F = 2(A_m \cdot \gamma_m + A_a \cdot \gamma_a + A_i \cdot \gamma_i) \quad (5)$$

where the subscripts m, a, and i stand for matrix, aggregate, and interface phases, respectively, and A is the area of the fracture surface and γ is the energy wasted for the crack propagation. In order to look into the rise in G_F , the fracture surface was examined. A MATLAB code was used to determine the area % of the various aggregate failure mechanisms. It is important to note that in RCA, mortar failure is defined as the fracture of mortar components, primarily the crushed mortar.

The area % of various aggregate failure types with varying FT cycles is displayed in Figures 8B

and C. Generally speaking, there is a discernible rise in interface damage (Figure 8C), which is correlated with a dramatic reduction in splitting damage (Figure 8B). The area percentages of interface failure (Figure 8C) and fractured aggregate (Figure 8B) were 7.3% and 18.5%, respectively, for the control specimen with zero FT cycle. Specimens exposed to 120 FT cycles in sulphate solution, however, displayed respective yields of 9.6% and 14.9%. The area percentages of splitting and pulled-out failure were around 5% and 17.3%, respectively, following 180 FT cycles. Comparing specimens treated to FT under sulphate exposure to those exposed to water, the former had a greater area % at all examined FT cycles for pulled-out aggregate failure. Following 180 FT cycles, the specimens exposed to sulphate had an area percentage of pulled-out aggregate failure of 22.1%, while the specimens exposed to water had an area percentage of 17.3%. This suggests that throughout the cyclic FT damage, there is a notable decline in the mortar's binding power. The collapse of the curved interface ultimately leads to a larger area of the fracture surface in comparison to the area of ligament. However, the effective cross-section area ($t \cdot h$) is used to determine the fracture energy, which results in a greater fracture energy.

3.5. The Connection between Damage Parameters and Strength

Understanding the deterioration of compressive strength under freeze-thaw cycles is crucial for the practical use of concrete in cold climates, given the compressive forces acting on structural concrete. Tensile strength is a fundamental metric in the fracture analysis and simulation of concrete structures. Therefore, assessing strength under FT cycles is essential, as it will aid in the creation of concrete performance models and service life tools, facilitating a comprehensive approach to degradation evaluation [43]. The strength loss and damage parameters for several FT cycles are illustrated in Figure 9. The damage parameter, compressive strength, and split-tensile strength exhibited a robust linear correlation with freeze-thaw cycles. Consequently, for a specific concrete exposed to freeze-thaw cycles, the damage parameter can be utilised to forecast the residual strength.

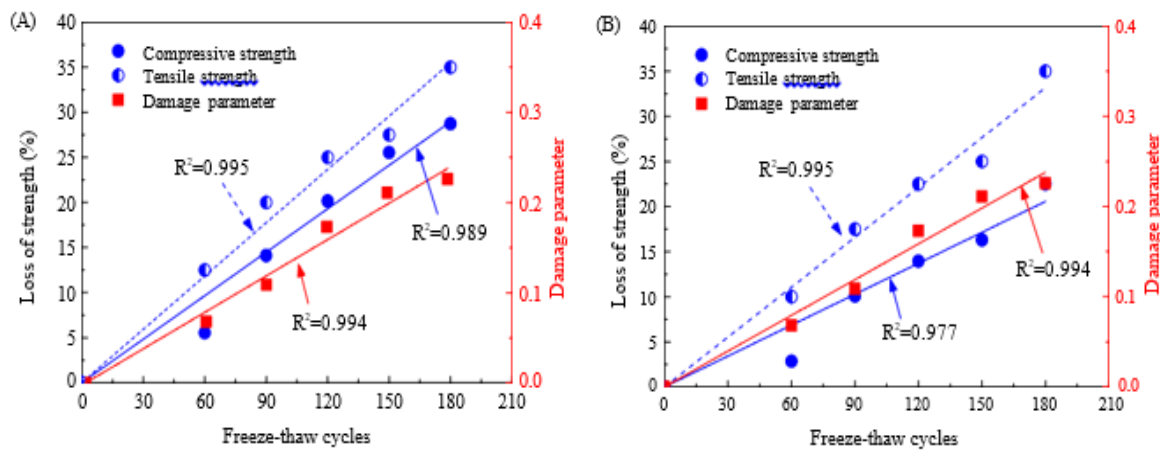


Figure 9. The relationship between strength loss and damage parameter for water-exposed (A) and sulphate-exposed (B) RAC.

For the specimen subjected to FT cycles, its residual strength can be expressed as;

$$\sigma_R = \sigma_0(1 - \alpha(1 - e^{\beta n})) \quad (6)$$

where σ_R and σ_0 denote the residual and original strength, respectively, and n represents the number of FT cycles in strength prediction. The coefficients α and β can be determined using Equations (7) and (8).

$$\alpha = (1 - \sigma_R(N)/\sigma_0)/(1 - E_{dyn,FT-N}/E_{dyn,0}) \quad (7)$$

and

$$\beta = \ln(E_{dyn,FT-N}/E_{dyn,0})/N \quad (8)$$

In this experiment, N represents the number of FT cycles, while $E_{dyn,0}$ and $E_{dyn,FT-N}$ denote the dynamic elastic modulus prior to and following FT tests with N cycles, respectively. The factor α , approximately equal to one, represents the relationship between strength deterioration and dynamic elastic modulus, while β denotes the impact of FT cycles on the dynamic elastic modulus. The dynamic elastic modulus has been extensively researched in relation to concrete with varying mixture properties, facilitating the determination of these coefficients. In the current study, the parameters $\alpha = 1.16$ and $\beta = 0.002$ can be employed to predict the residual compressive strength of specimens exposed to water-saturated freeze-thaw conditions.

3.6 Analytical Techniques

Any potential products formed from the chemical attack were further analysed using XRD. Freeze-thaw damage in water-saturated concrete constitutes a process of physical degradation. Therefore, only the specimen exposed to sulphate was analysed using XRD. Figure 10 displays the XRD patterns for specimens 0 and S150. The XRD pattern of S150 exhibited the presence of calcium carbonate. The decomposition of thaumasite occurs at approximately 60 °C during oven drying treatment. The prominence of ettringite was more pronounced in specimen S150, suggesting that ettringite serves as a corrosion product. XRD analysis indicates that chemical sulphate attack occurs in the FT tests subjected to sulphate solution exposure. Thaumasite and ettringite are formed in specimens subjected to sulphate attack. The lower temperature may considerably reduce the reaction rate between sulphate ions and hydration products; however, this chemical attack must still be considered in the long-term performance of RAC.

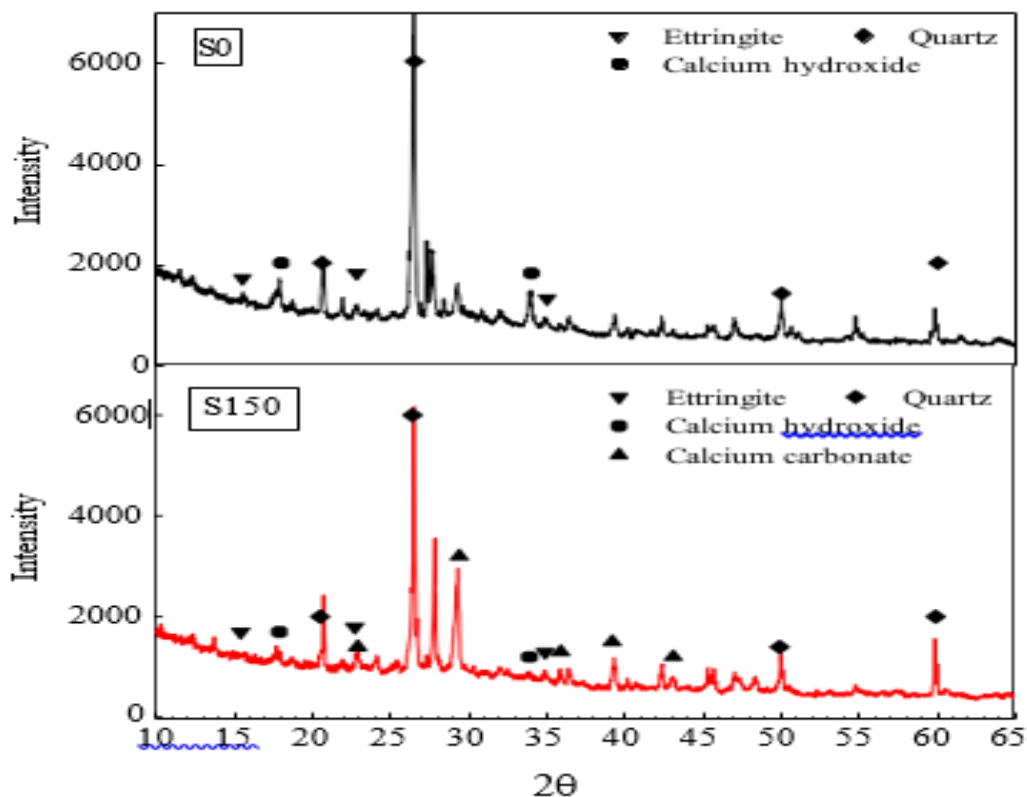


Figure 10 presents the XRD patterns of RAC under control conditions (S0) and after exposure to sulphate during FT cycles (S150).

4. Conclusion

This study investigates the effects of FT damage on the mechanical properties of high-performance RAC. Conditions involving exposure to both water and sulphate were examined. The results indicate the following conclusions:

The mass of the oven-dried sample decreases linearly with the number of freeze-thaw cycles. The saturated mass exhibits minor fluctuations throughout the tests. The loss of the oven-dried mass is a more appropriate measure for evaluating FT damage compared to the saturated mass. The water-exposed freeze-thaw cycles lead to greater deterioration in mass loss, elastic modulus, and compressive strength, whereas the sulphate-exposed freeze-thaw cycles result in more significant degradation of splitting tensile strength and fracture energy. The deterioration in splitting tensile strength is more pronounced than that of compressive strength. The maximum reductions in compressive and splitting tensile strength are 28.7% and 35%, respectively. The fracture energy exhibited an initial increase up to 60 freeze-thaw cycles, subsequently declining by 180 cycles. The results showed a maximum increase of approximately 45% for water-exposed samples and 39% for sulfate-exposed samples after undergoing 60 freeze-thaw cycles. The examination of failure modes in coarse aggregate indicates that FT damage leads to a notable decline in the binding strength of mortar. Following 180 FT cycles, the area percentage of pulled-out failure increased from 7.3% to over 17.3%.

References

1. Meyer, C. The greening of the concrete industry. *Cem. Concr. Compos.* **2009**, *31*, 601–605.
2. Faella, C.; Lima, C.; Martinelli, E.; Pepe, M.; Realfonzo, R. Mechanical and durability performance of sustainable structural concretes: An experimental study. *Cem. Concr. Compos.* **2016**, *71*, 85–96.
3. Va'zquez, E. *Progress of Recycling in the Built Environment*; Springer: Berlin/Heidelberg, Germany, 2013.
4. Hasanbeigi, A.; Price, L.; Lin, E. Emerging energy-efficiency and CO₂emission-reduction technologies for cement and concrete production: A technical review. *Renew. Sustain. Energy Rev.* **2012**, *16*, 6220–6238.
5. Behera, M.; Bhattacharyya, S.K.; Minocha, A.K.; Deoliya, R.; Maiti, S. Recycled aggregate from C&D waste & its use in concrete—A breakthrough towards sustainability in construction sector: A review. *Constr. Build. Mater.* **2014**, *68*, 501–516.
6. Amario, M.; Rangel, C.S.; Pepe, M.; Toledo Filho, R.D. Optimization of normal and high strength recycled aggregate concrete mixtures by using packing model. *Cem. Concr. Compos.* **2017**, *84*, 83–92.
7. Santana Rangel, C.; Amario, M.; Pepe, M.; Yao, Y.; Mobasher, B.; Toledo Filho, R.D. Tension stiffening approach for interface characterization in recycled aggregate concrete. *Cem. Concr. Compos.* **2017**, *82*, 176–189.
8. Dong, W.; Wu, Z.; Zhou, X.; Dong, L.; Kastiukas, G. FPZ evolution of mixed mode fracture in concrete: Experimental and numerical. *Eng. Fail. Anal.* **2017**, *75*, 54–70.
9. Bui, N.K.; Satomi, T.; Takahashi, H. Improvement of mechanical properties of recycled aggregate concrete basing on a new combination method between recycled aggregate and natural aggregate. *Constr. Build. Mater.* **2017**, *148*, 376–385.
10. Bravo, M.; de Brito, J.; Evangelista, L.; Pacheco, J. Superplasticizer's efficiency on the mechanical properties of recycled aggregates concrete: Influence of recycled aggregates composition and incorporation ratio. *Constr. Build. Mater.* **2017**, *153*, 129–138.
1. Pepe, M.; Toledo Filho, R.D.; Koenders, E.A.B.; Martinelli, E. A novel mix design methodology for Recycled Aggregate Concrete. *Constr. Build. Mater.* **2016**, *122*, 362–372.
2. Dilbas, H.; Sims,ek, M.; Çakir, Ö. An investigation on mechanical and physical properties of recycled aggregate concrete (RAC) with and without silica fume. *Constr. Build. Mater.* **2014**, *61*, 50–59.
3. Mehta, P.K.; Monteiro, P.J.M. *Concrete: Microstructure, Properties and Materials*; McGraw Hill: New York, NY, USA, 2006.
4. Li, W.; Pour-Ghaz, M.; Castro, J.; Weiss, J. Water Absorption and Critical Degree of Saturation Relating to Freeze-Thaw Damage in Concrete Pavement Joints. *J. Mater. Civ. Eng.* **2012**, *24*, 299–307.
5. Kou, S.C.; Poon, C.S. Effect of the quality of parent concrete on the properties of high performance recycled aggregate concrete. *Constr. Build. Mater.* **2015**, *77*, 501–508.
6. Bulatovic, V.; Melešev, M.; Radeka, M.; Radonjanin, V.; Lukic, I. Evaluation of sulfate resistance of concrete with recycled and natural aggregates. *Constr. Build. Mater.* **2017**, *152*, 614–631.
7. Kwan, W.H.; Ramli, M.; Kam, K.J.; Sulieman, M.Z. Influence of the amount of recycled coarse

- aggregate in concrete design and durability properties. *Constr. Build. Mater.* **2012**, 26, 565–573.
8. Gomes, M.; De Brito, J. Structural concrete with incorporation of coarse recycled concrete and ceramic aggregates: Durability performance. *Mater. Struct.* **2009**, 42, 663–6675.
 9. Levy, S.M.; Helene, P. Durability of recycled aggregates concrete: A safe way to sustainable development. *Cem. Concr. Res.* **2004**, 34, 1975–1980.
 10. Bassuoni, M.T.; Nehdi, M.L. Durability of self-consolidating concrete to sulfate attack under combined cyclic environments and flexural loading. *Cem. Concr. Res.* **2009**, 39, 206–226.
 11. Zeng, Q.; Fen-Chong, T.; Li, K. Freezing behavior of cement pastes saturated with NaCl solution. *Constr. Build. Mater.* **2014**, 59, 99–110.
 12. Liu, Z.; Hansen, W. Freeze–thaw durability of high strength concrete under deicer salt exposure. *Constr. Build. Mater.* **2016**, 102, 478–485.
 13. Sun, Z.; Scherer, G.W. Effect of air voids on salt scaling and internal freezing. *Cem. Concr. Res.* **2010**, 40, 260
 14. Farnam, Y.; Wiese, A.; Bentz, D.; Davis, J.; Weiss, J. Damage development in cementitious materials exposed to magnesium chloride deicing salt. *Constr. Build. Mater.* **2015**, 93, 384–392.
 15. Wan, X.S.; Lai, Y.M. Experimental study on freezing temperature and salt crystal precipitation of sodium sulphate solution and sodium sulphate saline soil. *Chin. J. Geotech. Eng.* **2013**, 35, 7. (In Chinese)
 16. Ghorbel, E.; Wardeh, G. Influence of recycled coarse aggregates incorporation on the fracture properties of concrete. *Constr. Build. Mater.* **2017**, 154, 51–60.
 17. Chen, G.M.; Yang, H.; Lin, C.J.; Chen, J.F.; He, Y.H.; Zhang, H.Z. Fracture behaviour of steel fibre reinforced recycled aggregate concrete after exposure to elevated temperatures. *Constr. Build. Mater.* **2016**, 128, 272–286.
 18. Gesoglu, M.; Güneyisi, E.; Öz, H.Ö.; Taha, I.; Yasemin, M.T. Failure characteristics of self-compacting concretes made with recycled aggregates. *Constr. Build. Mater.* **2015**, 98, 334–344.
 19. Guo, Y.C.; Zhang, J.H.; Chen, G.; Chen, G.M.; Xie, Z.H. Fracture behaviors of a new steel fiber reinforced recycled aggregate concrete with crumb rubber. *Constr. Build. Mater.* **2014**, 53, 32–39.
 20. *GB/T 50082-2009*; Standard for Test Methods of Long-Term Performance and Durability of Ordinary Concrete. Ministry of Housing and Urban-Rural Development: Beijing, China, 2009. (In Chinese)
 21. Abbaszadeh, R.; Modarres, A. Freeze-thaw durability of non-air-entrained roller compacted concrete designed for pavement containing cement kiln dust. *Cold Reg. Sci. Technol.* **2017**, 141, 16–27.
 22. Liu, Z.; Hansen, W. Pore damage in cementitious binders caused by deicer salt frost exposure. *Constr. Build. Mater.* **2015**, 98, 204–216.
 23. Jin, S.; Zheng, G.; Yu, J. A micro freeze-thaw damage model of concrete with fractal dimension. *Constr. Build. Mater.* **2020**, 257, 119434.
 24. Eriksson, D.; Wahlbom, D.; Malm, R.; Fridh, K. Hygro-thermo-mechanical modeling of partially saturated air-entrained concrete containing dissolved salt and exposed to freeze-thaw cycles. *Cem. Concr. Res.* **2021**, 141, 106314.
 25. RILEM Draft Recommendation (TC50-FMC). Determination of fracture energy of mortar and concrete by means of three-point bend test on notched beams. *Mater. Struct.* **1985**, 18, 285–290.
 26. *GB/T 50081-2002*; Standard for Test Method of Mechanical Properties on Ordinary Concrete. Ministry of Housing and Urban-Rural Development: Beijing, China, 2002. (In Chinese)
 27. Kequan, Y.; Jiangtao, Y.; Zhoudao, L.; Qingyang, C. Determination of the softening curve and fracture toughness of high-strength concrete exposed to high temperature. *Eng. Fract. Mech.* **2015**, 149, 156–169.
 28. Neville, A. The confused world of sulfate attack on concrete. *Cem. Concr. Res.* **2004**, 34, 1275–1296.
 29. Whittaker, M.; Black, L. Current knowledge of external sulfate attack. *Adv. Cem. Res.* **2015**, 27, 532–545.
 30. Lothenbach, B.; Bary, B.; Le Bescop, P.; Schmidt, T.; Leterrier, N. Sulfate ingress in Portland cement. *Cem. Concr. Res.* **2010**, 40, 1211–1225.
 31. Jiang, L.; Niu, D.; Yuan, L.; Fei, Q. Durability of concrete under sulfate attack exposed to freeze–thaw cycles. *Cold Reg. Sci. Technol.* **2015**, 112, 112–117.